Research Square

Preprints are preliminary reports that have not undergone peer review.
They should not be considered conclusive, used to inform clinical practice,
or referenced by the media as validated information.

Comprehensive characterization of N-lactoyl-amino acids as novel endogenous metabolites across diverse biological matrices

Jiahui Wang
Academy of Life and Natural Sciences, Xi'an Jiaotong- Liverpool University
Zhichao Zhang
Academy of Life and Natural Sciences, Xi'an Jiaotong- Liverpool University
Zheng Pang
Academy of Life and Natural Sciences, Xi'an Jiaotong- Liverpool University
Weiding Wang
Academy of Life and Natural Sciences, Xi'an Jiaotong- Liverpool University
Yan Liu
Sun Yat-sen University
Qingyang Wu
Academy of Life and Natural Sciences, Xi'an Jiaotong- Liverpool University
Anxin Wang
Beijing Neurosurgical Institute, Capital Medical University
Qian Zhang
Academy of Life and Natural Sciences, Xi'an Jiaotong-Liverpool University
Lei Fu
Academy of Life and Natural Sciences, Xi'an Jiaotong- Liverpool University
Ken Cheng
ken.cheng@xjtlu.edu.cn

Academy of Life and Natural Sciences, Xi'an Jiaotong- Liverpool University

Article

Keywords: N-lactoyl-amino acids (Lac-AAs), N-lactoyl-aromatic amino acids (Lac-AAAs), N-lactoyl-branched-chain amino acids (Lac-BCAAs), quantitative mass spectrometry, tissue-specific distribution

Posted Date: November 25th, 2026

DOI: https://doi.org/10.21203/rs.3.rs-11758116/v1

License: This work is licensed under a Creative Commons Attribution 4.0 International License.
Read Full License

Additional Declarations: No competing interests reported.

Abstract

N-lactoyl-amino acids (Lac-AAs) are endogenous metabolites implicated in appetite regulation, energy homeostasis, and metabolic disorders. However, current research has mainly focused on *N*-lactoyl-phenylalanine and has primarily relied on untargeted, non-quantitative analytical approaches, limiting a comprehensive understanding of Lac-AAs and their potential clinical applications. This study aimed to systematically identify and quantitatively characterize endogenous Lac-AAs across multiple biological matrices and in a human cohort, and to explore their associations with metabolic phenotypes in human, animal, and cell models. Eleven high-purity Lac-AAs identified by untargeted metabolomics in pooled human plasma were chemically synthesized, and a targeted HPLC-MRM-MS/MS method was established for their quantitative analysis in human serum, mouse tissues, and STC-1 cells. Circulating Lac-AAs, particularly *N*-lactoyl-branched-chain amino acids (Lac-BCAAs) and *N*-lactoyl-aromatic amino acids (Lac-AAAs), were highly intercorrelated and significantly associated with BMI and triglycerides. Distinct tissue-specific distribution patterns were identified in mice, with marked enrichment of Lac-AAAs and Lac-BCAAs in the small intestine of mice with hepatic steatosis, which was further supported in OA-treated STC-1 cells. Collectively, this work provides the first comprehensive quantitative characterization of endogenous Lac-AAs across multiple biological matrices and demonstrates their associations with metabolic disorder-related features, providing a quantitative foundation for future mechanistic investigation.

1. Introduction

N-lactoyl-amino acids (Lac-AAs) are a group of endogenous pseudo-dipeptides synthesized from lactate and amino acids via the reverse catalytic action of the protease cytosolic nonspecific dipeptidase 2 (CNDP2) [1]. This class of metabolites was first identified in 2015 by Jansen et al., who observed significant enrichment of several Lac-AAs in the culture medium of HEK 293 cells overexpressing the human orphan transporter ABCC5 [1]. Their biosynthetic pathway was subsequently elucidated using an integrated approach combining untargeted metabolomics and fractionated proteomics [1]. To date, largely owing to their low natural abundance, only six Lac-AAs have been reported across five published studies [1–5], including *N*-lactoyl-isoleucine (Lac-Ile), *N*-lactoyl-leucine (Lac-Leu), *N*-lactoyl-phenylalanine (Lac-Phe), *N*-lactoyl-tyrosine (Lac-Tyr), *N*-lactoyl-tryptophan (Lac-Trp), and *N*-lactoyl-valine (Lac-Val). While several recent studies have predominantly focused on Lac-Phe, these investigations have largely relied on untargeted metabolomics and lack rigorous quantitative validation [5–9]. **Consequently, the concentration profiles and broader biological functions of Lac-AAs remain poorly characterized and warrant further comprehensive investigation.**

Lac-AAs, particularly Lac-Phe, are emerging as crucial biomarkers for metabolic disorders. The latest research has established strong associations between circulating Lac-Phe levels and several metabolic conditions, including obesity [6,7,9], insulin resistance [5,8,10], type 2 diabetes [4,5,8,10,11], and mitochondrial-related diseases [2,3]. For instance, a large cross-sectional cohort study from the Qatar Biobank (n = 2,918)

found that individuals with insulin resistance and diabetic complications had elevated levels of Lac-Phe, Lac-Tyr, and Lac-Val. These Lac-AAs demonstrated strong positive correlations with key indicators of poor glycemic control, including HOMA-IR, glucose, and HbA1c, independently of metformin use [10]. In addition, a follow-up study from the IMI-DIRECT cohort (n = 3,000) identified plasma levels of Lac-Val, Lac-Leu, and lactate as strongly associated with the progression rate of HbA1c, serving as significant mediators of T2D progression from baseline to 18- and 48-month follow-up [4].

Beyond their role as biomarkers for metabolic syndromes, Lac-Phe has also demonstrated rapid and dynamic responses to various physiological and pharmacological stimuli, including food intake [6,8], physical exercise [6,7], and the administration of hypoglycemic agents such as metformin [5,8]. For example, Li et al. (2022) reported that plasma Lac-Phe levels in mice and racehorses rose immediately after a single bout of running and returned to baseline within one hour post-exercise [6]. Similarly, metformin administration led to an approximately two-fold increase in circulating Lac-Phe levels in both human and mouse models. The elevation was linked to a subsequent reduction in food intake and improvements in body weight and glucose homeostasis [5,8]. Emerging evidence indicates that Lac-Phe can directly influence cellular lipid metabolism [12]. In particular, Ying et al. showed that Lac-Phe treatment reduced lipid droplet accumulation in macrophages and promoted lipid metabolic reprogramming via the AMPK–PGC1α–PPARγ signaling axis, while simultaneously downregulating lipid-storage proteins such as PLIN2 and CD36. These findings provide the first cellular evidence that Lac-AAs species can regulate lipid metabolic processes. **These findings collectively suggest that Lac-Phe functions as a metabolic signaling molecule in regulating energy homeostasis and glucose-lipid metabolism. However, the precise molecular mechanisms underlying its physiological and pathophysiological roles remain to be fully elucidated.**

A 2024 study published in *Nature Metabolism* revealed that intestinal epithelial CNDP2^{+} cells, rather than macrophages, are the primary *in vivo* source of both basal and metformin-induced Lac-Phe production [8]. These findings highlight that the biological functions of Lac-AAs in host metabolism are likely to be tissue-specific, underscoring the need for a systematic characterization of their distribution and physiological relevance.

Therefore, **the primary objective of the present study** was to systematically characterize the presence, tissue-specific distribution, and metabolic relevance of endogenous Lac-AAs across multiple biological systems. To achieve this, eleven Lac-AAs identified by untargeted metabolomics were chemically synthesized as analytical standards, and a targeted HPLC-QQQ MS/MS method based on multiple reaction monitoring (MRM) was established for their quantitative analysis. Using this approach, we profiled Lac-AAs in human serum and across multiple tissues in fatty liver mice, examined their responses to metabolic stress in a cellular model, and explored their associations with metabolic phenotypes.

2. Materials and Methods

2.1. Chemicals and reagents

L-alanine benzyl ester hydrochloride was purchased from Aladdin (Beijing, China). *L*-tyrosine benzyl ester hydrochloride was obtained from Macklin (Shanghai, China). The other amino acid derivatives were acquired from Adamas (Shanghai, China), including *L*-alanine methyl ester hydrochloride, *L*-arginine methyl ester dihydrochloride, *L*-asparagine tert-butyl ester, *L*-aspartic acid dimethyl ester hydrochloride, *L*-cysteine methyl ester hydrochloride, *L*-glutamic acid dimethyl ester hydrochloride, *L*-glutamine tert-butyl ester hydrochloride, glycine methyl ester hydrochloride, *L*-histidine methyl ester dihydrochloride, *L*-isoleucine methyl ester hydrochloride, *L*-leucine methyl ester hydrochloride, *L*-lysine methyl ester hydrochloride, *L*-methionine methyl ester hydrochloride, *L*-phenylalanine methyl ester hydrochloride, *L*-proline methyl ester hydrochloride, *L*-serine methyl ester hydrochloride, *L*-threonine methyl ester hydrochloride, *L*-tryptophan methyl ester hydrochloride, *L*-tyrosine methyl ester hydrochloride, and *L*-valine methyl ester hydrochloride.

Acetonitrile (ACN) and formic acid were obtained from Thermo Fisher Scientific (MA, USA). Bovine serum albumin (BSA) was sourced from Beyotime (Beijing, China). Dichloromethane (DCM), N-ethyl-diisopropylamine, 1-ethyl-3-(3-dimethylaminopropyl)carbodiimide (EDCI), 1-hydroxybenzotriazole (HOBt), benzotriazol-1-yl-oxytripyrrolidinophosphonium hexafluorophosphate (PyBOP), N,N'-dicyclohexylcarbodiimide (DCC), *L*-lactic acid, activated carbon-supported palladium (Pd/C), and tetrahydrofuran (THF) were purchased from Adamas (Shanghai, China). Ethanol was obtained from Greagent (Shanghai, China). Methanol-d4 (CD_3OD), dimethyl sulfoxide-d6 (DMSO-d6), and chloroform-d ($CDCl_3$) were sourced from Macklin (Shanghai, China). Phosphate-buffered saline (PBS) came from Solarbio Science & Technology (Beijing, China), and lithium hydroxide monohydrate ($LiOH·H_2O$) was supplied by Adamas (Shanghai, China).

2.2. Untargeted serum metabolomic profiling for Lac-AAs detection

To identify the species of Lac-AAs present in biological samples, an untargeted metabolomics was performed on a pooled human serum sample using HPLC-QToF MS/MS (1290II-6530, Agilent, Santa Clara, CA, USA) in full-scan mode (m/z 50–500), as previously described with modification [13]. Briefly, serum proteins were precipitated, and metabolites were extracted with a mixture of ACN and MeOH (9:1, *v/v*). Chromatographic separation was carried out on a C18 column (100×2.1 mm, 2.2 μm, Acclaim, Thermo, Waltham, MA, USA) for a mobile phase consisting of (A) 0.1% formic acid in H_2O and (B) 0.1% formic acid in ACN. The gradient was programmed as follows: 0–1 min, 5% B; 1–8 min, 5%-55% B; 8–13 min, 55%-100% B; 13-16min, 100% B; 16–18 min, 100%-5% B; 18–20 min, 5% B, at a constant flow rate of 0.4 mL/min. Electrospray ionization (ESI) was operated in both positive and negative modes under the following conditions: gas temperature 350°C, drying gas flow rate 10 L/min, nebulizer pressure 45 psi, sheath gas temperature 350°C, sheath gas flow rate 11 L/min, and collision energy 10 eV. Data were collected using Masshunter Data Acquisition software (Agilent), and extracted ion chromatograms (EIC) of potential Lac-AAs were manually reviewed using ± 20 ppm and symmetric in Masshunter Qualitative

Analysis 10.0. The EIC with a single, symmetric peak shape and an intensity above 1×10^3 was defined as detected.

2.3. Procedures for synthesizing Lac-AAs standards

Amide bond formation between the carboxylic acid moiety of lactate and the amino functionality of the amino acid component in the Lac-AAs construct was achieved using sodium lactate in combination with amino acids protected as their methyl or benzyl derivatives. Lac-AAs, including Lac-Ile, Lac-Leu, Lac-Phe, Lac-Trp, Lac-Val, *N*-lactoyl aspartic acid (Lac-Asp), *N*-lactoyl glutamic acid (Lac-Glu), and *N*-lactoyl methionine (Lac-Met), were synthesized through the reaction of lactate with methylated amino acids. Figure 1A shows the reaction scheme of synthesizing Lac-Phe as an example. To produce methyl-protected Lac-AAs as a middle product, methyl-protected *L*-amino acid (1 equivalent), *L*-sodium lactate (2 equivalents), EDCI (2 equivalents), and HOBt (1 equivalent) were dissolved in DCM and stirred at room temperature for 28 h. After evaporation of the solvent, the crude product was dissolved in a mixture of THF and water containing LiOH (1.5 equivalents), and the mixture was stirred for 24 h to obtain the crude Lac-AAs. The crude Lac-AAs were crudely purified by column chromatography using chloroform and methanol as eluents. Fractions eluted with 6% methanol in chloroform were collected and concentrated under reduced pressure to yield the final Lac-AAs.

The Lac-AAs, including Lac-Tyr, *N*-lactoyl alanine (Lac-Ala), and *N*-lactoyl glycine (Lac-Gly), were synthesized through the reaction of lactate with benzylated amino acids. Figure 1B shows the Lac-Tyr synthesis scheme as an example. To produce benzyl-protected Lac-AAs as an intermediate product, benzyl-protected *L*-amino acid (1 equivalent), *L*-sodium lactate (2 equivalents), EDCI (2 equivalents), and HOBt (1 equivalent) were dissolved in DCM and stirred at room temperature for 28 h. After evaporation of the solvent, the crude product from the first step was combined with 10% (by weight) Pd/C in a mixture of DCM, ethanol, and water (10:12:4, v/v/v) under an H_2 atmosphere and stirred for 24 h to obtain the crude Lac-AAs. The crude Lac-AAs were crudely purified by column chromatography using chloroform and methanol as the eluent. Fractions eluted with 6% methanol in chloroform were collected and concentrated under reduced pressure to yield the final Lac-AAs.

For both synthesis routes, the final product was redissolved in acidified deionized water containing 1 M HCl to a pH = 2, and the mixture was extracted with ethyl acetate. The organic layer was then washed sequentially with brine and dried over anhydrous sodium sulfate (Na_2SO_4) to obtain the stable form. After filtration and concentration, the crude product was re-dissolved in a small amount of ethyl acetate and recrystallized by adding 10 mL of hexane. The isolated and dried crystals are collected as the final product.

Thin-layer chromatography (TLC) was performed to monitor reaction progress, and a silica gel column was used for purification with a mixture of DCM and MeOH as the eluent.

2.4. Lac-AAs standards purification and characterization

The synthesized Lac-AAs were purified by preparative HPLC (1260, Agilent, Santa Clara, CA, USA) equipped with a ZORBAX RX-SIL column (9.4 mm × 250 mm, 5 μm, Agilent), following established protocols [14]. The structures of these synthesized compounds were further characterized by proton nuclear magnetic resonance spectroscopy (^{1}H NMR, 600 MHz, Avance NEO, Bruker, Billerica, MA, USA) and high-resolution mass spectrometry (1290 II HPLC-6530 QToF MS/MS, Agilent). The final product purity was determined by analytical HPLC (1260, Agilent) coupled to a ZORBAX SB-Aq column (4.6 mm × 250 mm, 5 μm, Agilent) and evaluated using normalized peak areas, as previously described by Han et al. (2025).

2.5. Development of an HPLC-QQQ MS/MS quantitative method using synthesized Lac-AAs standards

A quantitative method for Lac-AAs was established using the synthesized Lac-AAs standards on an HPLC-QQQ MS/MS system (Triple Quad™ 6500+, ABSciex, Framingham, MA, USA) with an IonDrive™ Turbo V ion source [15]. The metabolites were quantified in MRM mode. Chromatographic separation was performed under the same column and mobile phase conditions as described for the untargeted profiling, with the following gradient: 0–3 min, 5% B; 3–7 min, 5%-45% B; 7–8 min, 50%-95% B; 8–9 min, 95% B, at a constant flow rate of 0.3 mL/min. Data was acquired in negative ESI mode with the following settings: curtain gas 25 psi, ion spray voltage − 4000 V, source temperature 300°C, ion source gas1 50 psi, ion source gas2 50 psi, declustering potential 50 V, collision gas medium, entrance potential − 10 V, and collision cell exit potential − 10 V. Detailed MRM transitions are listed in **Supplementary Table S1**.

2.6. Human serum samples from a Chinese cohort

Human serum samples (n = 649) were derived from the Kailuan cohort (ethical approval no. KS-2006-5), a population-based study conducted at Qianjiaying Hospital in Tangshan, China, as previously described [15]. The study was performed in compliance with the Declaration of Helsinki, and written informed consent was obtained from all participants. Cohort establishment, participant enrollment, and the collection, processing, aliquoting, and long-term storage of serum samples and associated clinical data were completed by the hospital clinical staff in 2016. The study was also approved by the Xi'an Jiaotong-Liverpool University Policy on Ethical Conduct in Research (ER-UEC-110000459202208171143 16).

The inclusion criteria were: (1) an age range of 30–65 years; and (2) stable body weight, defined as a change of less than 10%, for at least 3 months prior to the study. Exclusion criteria included: (1) a history of malignant tumors; (2) severe liver or kidney disease; (3) chronic hepatitis; (4) thyroid disease; (5) autoimmune disorders; (6) cardiovascular or cerebrovascular disease; and (7) pregnancy or lactation in women. Further details regarding the Kailuan cohort design have been described previously [16].

2.7. Diet-induced fatty liver mouse model

Animal experiments were conducted in specific-pathogen-free (SPF)-grade animal facilities at the CAM-SU Genomic Resource Center, Soochow University (Suzhou, China). Male C57BL/6J mice (8-week-old, n = 5/group) were housed under controlled conditions (20–26°C, 40%-70% relative humidity, and 12h

light/dark cycle). An obese phenotype was induced by feeding a high-fat, high-carbohydrate diet (HFHC, Noblebio, Shanghai, China) for 22 weeks. At the study endpoint, mice were fasted overnight and anesthetized with isoflurane or sevoflurane via inhalation. Mice's body weights were first measured. Blood samples were collected via orbital sinus puncture, after which the animals were euthanized by carbon dioxide inhalation. Tissue samples, including brain, brown adipose tissue (BAT), distal colon, inguinal white adipose tissue (iWAT), liver, kidney, pancreas, proximal colon, quadriceps muscle (QU), small intestine, and tibialis anterior muscle (TA), were rapidly dissected. Intestinal segments were defined according to established anatomical criteria[17,18]. All tissue samples were rinsed in PBS before snap-freezing. Serum samples were collected after centrifugation at 3000 *g* for 15 min at 4°C. All samples were snap-frozen in liquid nitrogen and stored at -80°C until further analysis.

All animal procedures were performed in accordance with the guidelines for the care and use of laboratory animals and were approved by the Institutional Animal Care and Use Committee of Soochow University (Approval No. KC-26-03) and the Ethics Committee of Xi'an Jiaotong-Liverpool University (Approval No. ER-SRR-11000045920240823180803).

2.8. H&E staining and triglyceride (TG) measurement in liver tissue

For H&E staining of liver sections, fresh liver tissues were fixed in 4% paraformaldehyde (Sangon Biotech, Shanghai, China) for at least 24 h. Samples were dehydrated through a graded ethanol series (70%, 80%, 90%, and 95%, 1 h each), followed by two changes of absolute ethanol for 30 min each. Tissues were subsequently cleared in xylene at 55°C for 40 min, infiltrated with molten paraffin at 80°C for at least 2 h, and embedded in paraffin. Paraffin blocks were sectioned at 3 μm using a Leica microtome, and sections were flattened in a 50°C water bath and dried at 65°C for 20 min. Sections were deparaffinized in xylene twice for 10 min each and rehydrated sequentially in absolute, 95%, 90%, and 80% ethanol for 3 min each, followed by rinsing in running tap water for 3 min. Sections were stained with hematoxylin (Jiuzhou Berlin Biotechnology, Beijing, China) for 3 min, rinsed for 1 min, differentiated in 1% acid alcohol for 1 s, and blued in water for 8 min. Sections were then counterstained with eosin (Jiuzhou Beilin Biotechnology) for 5 s. After staining, sections were dehydrated in 80%, 90%, and 95% ethanol for 30 s each, followed by absolute ethanol twice for 1 min each, cleared in xylene for 3 min, and mounted with neutral resin. Histological images were acquired using a Nikon inverted light microscope. Hepatic steatosis was histologically evaluated based on hepatocellular vacuolation and alterations in liver architecture. Hepatic lipid accumulation was further assessed by measuring TG levels using a commercial TG assay kit (Jiancheng Bioengineering Institute, Nanjing, China).

2.9. Enteroendocrine cell culture

Murine enteroendocrine STC-1 cells were purchased from Shanghai Fuheng Biotechnology (China). Cells were seeded in a 6-well plate with a density of 2×10^5 per well, and cultured in Dulbecco's modified Eagle's medium (DMEM) supplemented with 10% fetal bovine serum (FBS, Excell, Shanghai, China) and 1% penicillin-streptomycin (100U/mL, Sigma-Aldrich, St. Louis, MO, USA) at 37°C in a humidified 5% CO_2

atmosphere for 12 hours. Prior to treatment, cells were synchronized by starvation in serum-free DMEM supplemented with 1% penicillin-streptomycin for 12 h. Subsequently, cells were treated for 24 h with either 10% bovine serum albumin (BSA) as a control or a mixture of oleic acid (OA) at final concentrations of 100 and 200 μM, respectively. After treatment, both culture media and cell lysates were collected and stored at -80°C for subsequent analysis.

Lipid accumulation in the cellular model was confirmed using an Oil Red O Staining kit (G1262, Solarbio life Sciences, Beijing, China) and a triglyceride (TG) assay kit (Jiancheng Bioengineering Institute, Nanjing, China), following the manufacturer's instructions[14].

2.10. Quantification of endogenous Lac-AAs across the biological matrices

For quantification of Lac-AAs, serum (50 μL), tissue (20 mg), and cell culture medium (150 μL) samples were extracted using an ACN:MeOH (9:1, *v:v*) mixture spiked with phenylalanine-d5 (200 ng/mL) as an internal standard. Samples were sonicated in an ice-water bath for 10 min to facilitate extraction, then centrifuged at 18,000 *g* for 15 min at 4°C. The supernatant was collected, dried in a SpeedVac concentrator (SPD140DDA, Thermo Fisher Scientific, Waltham, MA, USA), and reconstituted in 50% ACN in H_2O for HPLC-QQQ MS/MS analysis as described in Section 2.5. Absolute quantification was performed using external standard calibration curves corrected for the internal standard, with Agilent MassHunter quantitative software. The Lac-AAs concentrations in serum and culture medium were expressed as ng/mL, whereas Lac-AAs levels in animal tissues were expressed as fold changes relative to the control group.

2.11. Statistical analysis

Cohort data analysis was conducted using R (v4.5.0), and statistical analyses of animal tissues and cell samples were performed using GraphPad Prism (v10).

Associations among the Lac-AAs and between Lac-AAs and clinical characteristics were assessed using Spearman's rank correlations. Waist-hip ratio (WHR) was calculated as waist circumference divided by hip circumference, and body mass index (BMI) was derived as weight (kg) divided by height squared (m^2). Outliers in numeric variables were identified based on the interquartile range (IQR) rule, defined as values below Q1 − 1.5×IQR or above Q3 + 1.5×IQR, and were treated as missing values separately for each variable. Correlation results were visualized using heatmaps and correlation plots with correlation coefficients (ρ) annotated, and statistical significance denoted by Benjamini-Hochberg false discovery rate (FDR)-adjusted *p* values (*< 0.05, **< 0.01, ***< 0.001).

Furthermore, for each metabolic phenotype, participants were classified into a Control group and a Metabolic Disorder group for comparative analysis. The diagnostic criteria were as follows: **Overweight** was defined as BMI ≥ 24 kg/m^2; **Fatty liver disease** was classified according to diagnoses made by cardiologists at secondary or tertiary hospitals; **Dyslipidemia** as meeting any of the following, total cholesterol (TC) ≥ 5.2 mmol/L, low-density lipoprotein cholesterol (LDL-c) ≥ 3.4 mmol/L, high-density

lipoprotein cholesterol (HDL-c) < 1.0 mmol/L, or triglycerides (TG) ≥ 1.7 mmol/L; **Hyperuricemia** as serum uric acid > 420 μmol/L in males or > 360 μmol/L in females; and **Hypertension** as systolic blood pressure ≥ 140 mmHg or diastolic blood pressure ≥ 90 mmHg. For all differential analyses between groups, missing values were addressed by restricting analyses to complete cases, retaining only participants with complete data for all variables included in each test.

Continuous variables are presented as median [Q1; Q3] along with the corresponding sample size (n). As the data were not normally distributed, between-group differences in Lac-AAs concentrations were assessed using the Wilcoxon rank-sum test. Effect sizes were quantified with Cliff's delta (Metabolic Disorder group − Control group; range: −1 to 1), where positive values indicate higher concentrations in the Metabolic Disorder group. To adjust for multiple comparisons across the Lac-AAs within each phenotype, *p*-values were adjusted using the FDR procedure. The results were visualized using violin plots overlaid with box plots.

To evaluate the associations between specific Lac-AAs and BMI, multivariable linear regression models were fitted with BMI as a continuous outcome and each Lac-AAs as the exposure of interest, adjusting for age and gender encoded as a binary variable. The analytical dataset was restricted to participants with data on BMI, age, gender, and Lac-AAs using complete-case analysis (n = 468, representing 72.1% of the original sample). No imputation methods were thus applied. To minimize potential multicollinearity among Lac-AAs, separate adjusted linear regression models were constructed for each Lac-AAs (BMI ~ Lac-AAs + age + gender). Lac-AAs concentrations were log-transformed prior to regression analysis to reduce right skewness. Regression coefficients (β), standard errors, 95% CIs, and *p* values were reported. Results were tabulated and ranked by FDR-adjusted *p*-value.

To assess the potential of Lac-AAs as biomarkers, we constructed logistic regression models using Lac-AAs that differed significantly among metabolic phenotypes. Receiver operating characteristic (ROC) curves were generated from model-predicted probabilities, and discriminatory performance was quantified by the area under the ROC curve (AUC). The cohort was randomly divided into training and validation sets using a stratified 70:30 split, with model development and variable selection performed in the training set and final model evaluation conducted in the validation set. Each Lac-AAs was first evaluated in a univariable logistic regression model, and the metabolite yielding the highest AUC was selected as the initial predictor. The remaining metabolites were then added individually to the current model, and the corresponding change in AUC was calculated. At each iteration, the metabolite producing the largest improvement in AUC was retained, provided that the absolute increase was at least 0.01. This procedure was repeated until no additional metabolite met the prespecified threshold. The dataset was randomly split 100 times, and a model was trained as described above for each split. Finally, the average AUC and confidence interval (CI) for all epochs will be reported.

3. Results

3.1. Chemical synthesis of Lac-AAs

To systematically profile this class of Lac-AAs metabolites in biological specimens, an untargeted metabolomics analysis was conducted on pooled human serum. By extracting targeted ion chromatograms from the full-scan data, 11 types of Lac-AAs were detected and subsequently selected for further synthesis in this study. The chromatographic results from untargeted metabolomics are presented in **Supplementary Fig. S1**.

The Lac-AAs standards were synthesized *via* a consistent two-step strategy. First, methylated or benzyl-protected amino acids were coupled with lactate. The resulting protected intermediates were then deprotected to yield the final products. The entire procedure was completed in approximately 52 hours, with the initial coupling and purification step taking about 28 hours and the second deprotection step taking about 24 hours. Using this approach, all 11 targeted Lac-AAs were successfully synthesized with high purity (90.00%- 99.99%; see **Supplementary Table S1** for details). These purified standards were subsequently employed to establish a quantitative analytical method using HPLC-QQQ MS/MS.

The corresponding structural validation and purity data for the remaining ten Lac-AAs are provided in **Supplemental Fig. S2**.

3.2. Association between Lac-AAs and clinical traits

Although **11** Lac-AAs were successfully synthesized, the structural isoforms Lac-Leu and Lac-Ile cannot be chromatographically resolved, and Lac-Gly cannot be consistently detected in all samples under the HPLC-QQQ MS/MS conditions used. Consequently, **nine** Lac-AAs metabolites were quantified in human serum samples (n = 649) from a community-based cohort.

Spearman correlation analysis revealed strong positive associations between circulating Lac-AAs levels and key clinical markers of metabolic disorders (Fig. 2A). Specifically, lactate-aromatic amino acids (Lac-AAAs: Lac-Phe, Lac-Trp, and Lac-Tyr) and lactate-branched-chain amino acids (Lac-BCAAs: Lac-Ile/Leu and Lac-Val) showed notable correlations with BMI, TG, and HDL. For BMI, the strongest correlations were observed with Lac-Tyr (ρ = 0.310), Lac-Ile/Leu (ρ = 0.303), Lac-Val (ρ = 0.239), Lac-Phe (ρ = 0.235), and Lac-Trp (ρ = 0.211; all $p < 0.001$). Regarding TG levels, Lac-Met (ρ = 0.389), Lac-Phe (ρ = 0.350), Lac-Ile/Leu (ρ = 0.345), Lac-Trp (ρ = 0.314), and Lac-Tyr (ρ = 0.217) showed relatively strong correlations (all $p < 0.001$). For HDL levels, significant correlations were found with Lac-Tyr (ρ = -0.218), Lac-Ile/Leu (ρ = -0.205), Lac-Val (ρ = -0.196), Lac-Phe (ρ = -0.151), Lac-Trp (ρ = -0.117), and Lac-Asp (ρ = 0.113; all $p < 0.001$). **Overall, Lac-AAs exhibited strong associations with key metabolic risk indicators, particularly BMI and TG.**

Inter-correlations among Lac-AAs were also examined (Fig. 2B). Strong positive correlations were observed within the Lac-AAAs, most notably between Lac-Phe and Lac-Trp (ρ = 0.843, $p < 0.001$). Lac-Phe also correlated positively with Lac-Tyr (ρ = 0.554, $p < 0.001$) and with Lac-Ile/Leu (ρ = 0.666, $p < 0.001$). Similarly, Lac-Tyr showed significant positive associations with Lac-Trp (ρ = 0.504, $p < 0.001$) and with Lac-Ile/Leu (ρ = 0.736, $p < 0.001$). In contrast, Lac-Val was negatively correlated with several other Lac-AAs, most distinctly with Lac-Met (ρ = -0.224, $p < 0.001$) and Lac-Phe (ρ = -0.122, $p < 0.01$). Lac-Asp

and Lac-Glu, which have negatively charged side chains, were moderately correlated with each other. **Together, these results reveal metabolite-specific correlation patterns among Lac-AAs, with the Lac-AAAs forming the most tightly coordinated cluster, suggesting potential coordinated regulation or metabolic pathways.**

3.3. Logistic regression-based diagnostic models

Candidate Lac-AAs were selected in the training set using a forward-selection procedure based on incremental improvements in AUC, and model performance was subsequently evaluated in the validation cohort across 100 repeated splits (Fig. 3A **and Supplementary Fig. S3**). The discriminatory performance was summarized by the mean validation AUC and the corresponding 95% repeated-split intervals. Among the evaluated phenotypes, **Fatty Liver Disease** showed the strongest discriminatory performance based on Lac-AAs profiles alone, with a mean validation AUC of **0.710** (95% repeated-split interval: **0.614–0.795**).

For Hyperuricemia, the Lac-AAs-based model achieved a mean validation AUC of **0.681** (95% repeated-split interval: **0.601–0.761**). **For Dyslipidemia**, it showed moderate discrimination, with a mean validation AUC of **0.650** (95% repeated-split interval: **0.572–0.720**), whereas **for Hypertension**, it showed a lower discriminatory ability with a mean validation AUC of **0.610** (95% repeated-split interval: **0.525–0.672**). The predictive performance **for Overweight** remained limited, with a mean validation AUC of **0.644** (95% repeated-split interval: **0.575–0.726**).

Overall, these exploratory analyses indicate that Lac-AAs profiles exhibit phenotype-dependent discriminatory capacity, with the strongest performance observed for **Fatty Liver Disease**. Incorporating additional clinical characteristics may further improve model performance and support future applications.

3.4. Elevated Lac-AAs in metabolic disorders

The Lac-AAs levels were also assessed under different metabolic disorder conditions. The results revealed that serum levels of Lac-Ile/Leu, Lac-Phe, Lac-Trp, and Lac-Tyr were significantly elevated in individuals with **Fatty Liver Disease**, **Dyslipidemia**, and **Hypertension** (all $p < 0.001$; **Supplementary Table S3**). Lac-Val levels were also higher in the **Overweight** and **Fatty Liver** groups. Lac-Asp, Lac-Glu, Lac-Tyr, Lac-Met, and Lac-Val levels were closely associated with **Hyperuricemia**.

Comparison of Lac-AAs concentrations between **Control** and **Fatty Liver** individuals (Fig. 3B) showed that Lac-AAAs (Lac-Phe, Lac-Trp, Lac-Tyr), Lac-BCAAs (Lac-Ile/Leu, Lac-Val), and Lac-Glu were significantly elevated in the **Fatty Liver group** (all $p < 0.001$), whereas no significant differences were observed for Lac-Ala, Lac-Met, and Lac-Asp. **Collectively, these results demonstrate that circulating levels of multiple Lac-AAs, particularly Lac-AAAs and Lac-BCAAs, are elevated in individuals with metabolic disorders, with the most pronounced alterations observed in those with fatty liver disease, suggesting potential associations between Lac-AAs dysregulation and metabolic disturbances.**

3.5. Lac-AAs distribution in tissues from fatty liver mice

To investigate the tissue-specific and metabolite-specific importance of Lac-AAs in fatty liver disease, targeted profiling of Lac-AAs was conducted in the tissues from **Control** and **Fatty Liver** mice, including BAT, brain, distal colon, iWAT, kidney, liver, pancreas, proximal colon, QU, small intestine, serum, and TA (Fig. 4).

Mice fed the HFHC diet exhibited a pronounced increase in body weight and hepatic fat accumulation over the 22-week intervention period. Histological examination and hepatic TG quantification confirmed the successful establishment of the fatty liver mouse model (**Supplementary Fig. S4**).

Compared with the normal diet group, alterations in Lac-AAs concentrations were consistently observed across multiple tissues in Fatty Liver mice, including iWAT, liver, small intestine, and serum (Fig. 4). Notably, the changes of Lac-AAs in the small intestine were the most pronounced (8 to 16-fold) in Fatty Liver mice. The fold changes of Lac-AAAs, including Lac-Phe, Lac-Trp, and Lac-Tyr in the small intestine, ranged from 1.5 to 4 times above the control levels. In addition, the BAT appears to be an important tissue for Lac-AAAs (Fig. 4A) and Lac-AAs with negatively charged side chains, including Lac-Asp and Lac-Glu (Fig. 4C). The proximal colon exhibits distinct levels of Lac-BCAAs, and the pancreas plays a crucial role in the changes of Lac-Asp and Lac-Glu.

Regarding Lac-AAs specificity, the metabolites were classified into four groups based on the properties of their amino acid side chains (Fig. 4). Among these categories, changes in Lac-AAAs (Lac-Phe, Lac-Trp, and Lac-Tyr) were the most predominant, followed by Lac-BCAAs (Lac-Ile/Leu and Lac-Val). For instance, Lac-AAAs levels increased by approximately 8-16-fold, and Lac-BCAAs showed moderate elevations of about 2-10-fold in iWAT, liver, and serum. In contrast, Lac-AAs with negatively charged side chains (Lac-Asp and Lac-Glu) exhibited smaller changes (1.5-3-fold range), while Lac-AAs with hydrophobic side chains (Lac-Ala and Lac-Met) displayed 1-2-fold alterations in these tissues. These differences are likely attributed to the distinct physicochemical properties of the amino acid side chains, which influence the biological formation, stability, tissue distribution, and metabolic turnover of individual Lac-AAs. **Collectively, these findings demonstrate metabolite-specific and tissue-dependent remodeling of Lac-AAs profiles in mice with fatty liver disease and suggest that the intestinal tract may be a major site for Lac-AAs accumulation or metabolism, although the underlying mechanisms require further investigation.**

3.6. Lac-AAs concentrations in fatty acid-treated enteroendocrine STC-1 cells

To further verify alterations in Lac-AAs concentrations in the small intestine under metabolic-disorder conditions, a murine enteroendocrine cell line, STC-1, was selected to establish an *in vitro* intestinal model treated with OA.

Oil Red O staining revealed a progressive accumulation of lipid droplets in STC-1 cells as OA concentration increased from 100 to 200 μM (Fig. 5A and 5B). Consistently, intracellular TG levels were also markedly elevated after OA treatment, confirming successful establishment of the lipid

accumulation model in STC-1 (Fig. 5C). Among the measured Lac-AAs (Fig. 5D), Lac-Phe, Lac-Trp, and Lac-Tyr were significantly increased in the 100 μM OA group, but not in the 200 μM OA group. Notably, Lac-Val levels were consistently elevated in both OA-treated groups. **These findings indicate that OA-induced lipid accumulation selectively reshapes Lac-AAs metabolism in STC-1 cells, suggesting that specific Lac-AAs, particularly Lac-AAAs, may contribute to metabolic dysregulation.**

4. Discussion

This study provides a systematic and comprehensive characterization of Lac-AAs, an emerging class of metabolites, by integrating chemical synthesis, targeted MS-based quantification, and biological analyses across multiple experimental systems. In total, 11 types of Lac-AAs, including Lac-Ala, Lac-Asp, Lac-Glu, Lac-Gly, and Lac-Trp, as well as five previously unreported compounds, were chemically synthesized and quantified using HPLC-QQQ MS/MS. This analytical framework enabled us to move beyond the predominant focus on Lac-Phe and to investigate Lac-AAs as a broader metabolite family across human, animal, and cellular systems.

Using this quantitative platform, analyses of the community-based Kailuan cohorts identified Lac-AAAs and Lac-BCAAs as the predominant Lac-AAs subclasses associated with metabolic disorders, particularly fatty liver. Their circulating levels were positively correlated with BMI, TG, fasting blood glucose, and obesity, with particularly strong associations observed among overweight individuals. These results suggest that Lac-AAAs and Lac-BCAAs may be sensitive indicators of disturbances in energy balance and glucose homeostasis. They are highly consistent with the recent findings of Xiao et al. (2024), who demonstrated that Lac-Phe is markedly elevated in obesity, insulin resistance, and T2D-related metabolic phenotypes and may serve as an important circulating marker of metabolic status [19]. However, compared with Lac-Phe, other Lac-AAAs and Lac-BCAAs remain substantially less studied. Notably, aromatic amino acids and branched-chain amino acids have long been linked to obesity, insulin resistance, and T2D, and their elevated circulating levels are widely regarded as early metabolic signatures of chronic energy surplus [15,20–22]. Thus, the lactoylation of these metabolically relevant amino acids may represent an additional layer of metabolic regulation that warrants further investigation.

Given the strong associations between circulating Lac-AAs and metabolic disorders, this study next explored whether Lac-AAs metabolism exhibited tissue specificity under metabolic stress. An HFHC diet-induced overweight mouse model was established, and Lac-AAs levels were compared across multiple tissues, including the BAT, brain, distal colon, iWAT, kidney, liver, pancreas, proximal colon, QU, small intestine, serum, and TA. Multiple Lac-AAs exhibited markedly higher levels in the small intestine than in other tissues, and the small intestine exhibited the most pronounced difference in Lac-AAs profiles between fatty liver and control mice. These findings suggest that the intestine may be a major site for Lac-AAs synthesis, accumulation, or metabolism. This observation is consistent with the findings of Li et al., who proposed the intestine as the primary source of endogenous Lac-AAs [23], and further supports a central role of the gut in Lac-AAs metabolism.

Based on this tissue-specific enrichment, an OA-treated intestinal enteroendocrine STC-1 cell model was further established. Most Lac-AAs showed an increasing trend following OA treatment, providing *in vitro* support for the association between lipid overload and altered Lac-AAs profiles observed *in vivo*. The intestine may therefore contribute to the relationship between Lac-AAs metabolism and systemic metabolic regulation. Recent work by Xiao et al., (2024) demonstrated that Lac-Phe can modulate the GDF25-GFRAL signaling pathway in the mouse intestine, which is implicated in energy balance and appetite control [19]. However, the present *in vitro* experiments were limited to STC-1 cells, a single intestinal enteroendocrine cell line. Future studies should include additional intestinal cell types, organoid models, and primary intestinal cells to capture potential heterogeneity in Lac-AAs synthesis, transport, signaling, and downstream metabolic effects.

Several limitations of this study should also be acknowledged. First, the selection of Lac-AAs was based on untargeted metabolomics results, which may have limited the detection of low-abundant Lac-AAs. Second, Lac-Ile and Lac-Leu were quantified as a combined chromatographic signal (Lac-Ile/Leu) because they could not be chromatographically resolved under the current analytical conditions. Consequently, the measured signal may mask individual differences between Lac-Ile and Lac-Leu. Previous studies have demonstrated distinct roles of leucine and isoleucine in metabolic regulation, insulin sensitivity, and energy homeostasis [24,25]. Future studies employing improved chromatographic separation and isomer-specific quantification will be required to clarify their respective biological functions. Accordingly, the present findings concerning Lac-BCAAs should be interpreted as reflecting the combined Lac-Ile/Leu signal rather than changes in either metabolite individually.

Although multiple Lac-AAs were altered in the small intestine under metabolic stress, their increased intestinal levels cannot be conclusively attributed to local synthesis, because changes in accumulation, transport, or degradation may also contribute. Stable isotope tracing, substrate flux analysis, and direct measurements of CNDP2 enzymatic activity under metabolic disorder conditions will be required to elucidate the mechanisms underlying tissue-specific Lac-AAs metabolism.

Finally, the absence of further increases in Lac-AAAs following treatment with 200 μM OA suggests that the Lac-AAs response to lipid overload may not be linearly dose-dependent. Excessive lipid exposure could trigger metabolic adaptation or pathway saturation. Alternatively, lipotoxicity at higher OA concentrations may contribute to the observed plateau in Lac-AAs levels[26], thereby limiting the further accumulation of specific Lac-AAs during prolonged metabolic stress. Similar adaptive metabolic remodeling has been reported under sustained nutrient excess[27,28]. However, because cell viability and relevant mechanistic parameters were not assessed in the present study, these explanations remain speculative and require further experimental validation.

5. Conclusion

This study presents the first comprehensive analysis of Lac-AAs, encompassing chemical synthesis, targeted quantification, and biological profiling across human, animal, and cellular systems. The

synthesis of 11 Lac-AAs standards has laid an analytical foundation for rigorous, quantitative studies of these metabolites in diverse biological matrices. Circulating Lac-AAs, particularly Lac-AAAs and Lac-BCAAs, were associated with key clinical indicators of metabolic disorders, including BMI, TG, fatty liver, and fasting blood glucose levels. Furthermore, Lac-AAs exhibit distinct tissue-specific distribution patterns, with the small intestine showing particularly pronounced alterations in Lac-AAAs levels under metabolic stress. The OA-treated STC-1 cell experiments further supported an association between lipid overload and altered Lac-AAs profiles. Overall, the current findings link Lac-AAs profiles to metabolic dysregulation and provide a quantitative basis for further studies investigating their sources, regulatory mechanisms, and potential biological functions.

Abbreviations

Full Name
ACN
Acetonitrile
BAT
Brown adipose tissue
BMI
Body mass index
BSA
Bovine serum albumin
$CDCl_3$
Chloroform-d
CD_3OD
Methanol-d4
DCM
Dichloromethane
DMSO-d6
Dimethyl sulfoxide-d6
EDCI
1-ethyl-3-(3-dimethylaminopropyl) carbodiimide
FDR
False discovery rate
HDL-c
High-density lipoprotein cholesterol
HOBt
1-Hydroxybenzotriazole
HPLC
High-performance liquid chromatography
iWAT

Inguinal white adipose tissue
LDL-c
Low-density lipoprotein cholesterol
Lac-AAAs
N-lactoyl-aromatic amino acid
Lac-AAs
N-lactoyl-amino acids
Lac-Ala
N-lactoyl-alanine
Lac-Asp
N-lactoyl-aspartic acid
Lac-BCAAs
N-lactoyl-branched-chain amino acids
Lac-Glu
N-lactoyl-glutamic acid
Lac-Gly
N-lactoyl-glycine
Lac-Ile
N-lactoyl-isoleucine
Lac-Leu
N-lactoyl-leucine
Lac-Met
N-lactoyl-methionine
Lac-Phe
N-lactoyl-phenylalanine
Lac-Trp
N-lactoyl-tryptophan
Lac-Tyr
N-lactoyl-tyrosine
Lac-Val
N-lactoyl-valine
$LiOH{\cdot}H_2O$
Lithium hydroxide monohydrate
MRM
Multiple reaction monitoring
OA
Oleic acid
PBS
Phosphate-buffered saline
PyBOP

Benzotriazol-1-yl-oxytripyrrolidinophosphonium hexafluorophosphate
QQQ
Triple quadrupole
QToF
Quadrupole time-of-flight
QU
Quadriceps muscle
STC-1
STC-1 enteroendocrine cells
TA
Tibialis anterior muscle
TC
Total cholesterol
TG
Triglyceride
THF
Tetrahydrofuran
TLC
Thin-layer chromatography
WHR
Waist-hip ratio

Declarations

Declaration of competing interest

The authors declare no conflicts of interest.

Ethical approval

All procedures performed in studies involving human participants were in accordance with the ethical standards of the institutional and/or national research committee and with the 1964 Declaration of Helsinki and its later amendments, or with comparable ethical standards. Informed consent was obtained from all individual participants included in the study. All procedures involving animal experiments were conducted in accordance with the Guidelines for the Care and Use of Laboratory Animals, and all efforts were made to minimize animal suffering.

Generative AI declaration

We declare that generative AI was not used for generating any scientific content of this manuscript. AI-assisted tools were used only for language polishing and improving readability.

Fundings

The research project was financially supported by the Young Scientists Fund of the National Natural Science Foundation of China (Grant No. 82404254), the Research Development Fund from Xi'an Jiaotong-Liverpool University (Grant number: RDF-21-02-069), and the SIP High-Quality Innovation Platform for Chronic Diseases (YZCXPT2022203).

Author Contribution

J.W. performed all experiments, including chemical synthesis, metabolite quantification and analysis, animal experiments, and cell experiments. J.W. also conducted data processing and analysis and drafted the original manuscript. Z.Z. was responsible for analyzing metabolomics data from the human cohort and generating the graphs. Q.Z. and W.W. developed the chemical synthesis methodologies and carried out the standard synthesis. Z.P. and Q.W. assisted in the accomplishment of animal experiments and sample collection. Y.L. and A.W. were responsible for the design of the human cohort, participant recruitment, and collection of samples and clinical data. L.F. provided analytical resources and study guidance. K.C. conceived and designed the overall study, supervised the project, and critically revised the manuscript. All authors reviewed and approved the final manuscript.

Acknowledgements

The authors thank all the research team members for their valuable contributions to this study, the technician staff at the mass spectrometry platform, and the animal facility for their assistance.

Data Availability

The data of this study are available within the article and its Supplementary materials. Additional datasets generated and analysed during the current study are available upon reasonable request.

References

1. Jansen, R. S. et al. N-lactoyl-amino acids are ubiquitous metabolites that originate from CNDP2-mediated reverse proteolysis of lactate and amino acids. *Proc. Natl. Acad. Sci. U.S.A.*112, 6601–6606 (2015).
2. Sharma, R. et al. Circulating markers of NADH-reductive stress correlate with mitochondrial disease severity. *J. Clin. Invest.* **131**, e136055 (2021).

3. Rogers, R. S. et al. Circulating N-lactoyl-amino acids and N-formyl-methionine reflect mitochondrial dysfunction and predict mortality in septic shock. *Metabolomics* **20**, 36 (2024).
4. Sharma, S. et al. Role of human plasma metabolites in prediabetes and type 2 diabetes from the IMI-DIRECT study. *Diabetologia* **67**, 2804–2818 (2024).
5. Scott, B. et al. Metformin and feeding increase levels of the appetite-suppressing metabolite Lac-Phe in humans. *Nat. Metab.* **6**, 651–658 (2024).
6. Li, V. L. et al. An exercise-inducible metabolite that suppresses feeding and obesity. *Nature* **606**, 785–790 (2022).
7. Hoene, M. et al. Exercise-Induced N-Lactoylphenylalanine Predicts Adipose Tissue Loss during Endurance Training in Overweight and Obese Humans. *Metabolites* **13**, 15 (2022).
8. Xiao, S. et al. Lac-Phe mediates the effects of metformin on food intake and body weight. *Nat. Metab.* **6**, 659–669 (2024).
9. Lund, J., Clemmensen, C. & Schwartz, T. W. Outrunning obesity with Lac-Phe? *Cell Metabol.* **34**, 1085–1087 (2022).
10. Naja, K. et al. N-lactoyl amino acids are potential biomarkers for insulin resistance and diabetic complications. *Diabetes Obes. Metabolism*. **27**, 5793–5804 (2025).
11. Xia, J. et al. Precise Metabolomics Defines Systemic Metabolic Dysregulation Distinct to Acute Myocardial Infarction Associated With Diabetes. *ATVB* **43**, 581–596 (2023).
12. Ying, W. et al. N-lactoyl-phenylalanine modulates lipid metabolism in microglia/macrophage via the AMPK-PGC1α-PPARγ pathway to promote recovery in mice with spinal cord injury. 1–20 10.1186/s12974-025-03495-3
13. Liu, T. et al. Postbiotic Limosilactobacillus reuteri cultured with Polygonatum kingianum polysaccharides ameliorates high-fat-high-sugar-deteriorated colitis and associated hepatobiliary disorders. *Int. J. Biol. Macromol.* **322**, 147065 (2025).
14. Han, Y. et al. A synthesis and quantification method for endogenous metabolites dimethylguanidino valeric acid. *Sci. Rep.* **15**, 11100 (2025).
15. Gar, C. et al. Serum and plasma amino acids as markers of prediabetes, insulin resistance, and incident diabetes. *Crit. Rev. Clin. Lab. Sci.* **55**, 21–32 (2018).
16. Liu, H. et al. Obesity and physical inactivity are associated with increased risks of cardiac conduction disease: a report from the Kailuan Cohort Study. *npj Cardiovasc. Health*. **1**, 9 (2024).
17. Mowat, A. M. & Agace, W. W. Regional specialization within the intestinal immune system. *Nat. Rev. Immunol.* **14**, 667–685 (2014).
18. Müller, A. K. et al. Olive oil extracts and oleic acid attenuate the LPS-induced inflammatory response in murine RAW264.7 macrophages but induce the release of prostaglandin E2. *Nutrients* **13**, 4437 (2021).
19. Xiao, S. et al. Lac-Phe mediates the effects of metformin on food intake and body weight. *Nat. Metab.* **6**, 659–669 (2024).

20. De Mello, V. D. et al. Serum aromatic and branched-chain amino acids associated with NASH demonstrate divergent associations with serum lipids. *Liver Int.* **41**, 754–763 (2021).
21. Zhang, L. & Han, J. Branched-chain amino acid transaminase 1 (BCAT1) promotes the growth of breast cancer cells through improving mTOR-mediated mitochondrial biogenesis and function. *Biochem. Biophys. Res. Commun.* **486**, 224–231 (2017).
22. Zhou, Y., Zhang, N., Arikawa, A. Y. & Chen, C. Inhibitory Effects of Green Tea Polyphenols on Microbial Metabolism of Aromatic Amino Acids in Humans Revealed by Metabolomic Analysis. *Metabolites* **9**, 96 (2019).
23. Li, V. L. et al. An exercise-inducible metabolite that suppresses feeding and obesity. *Nature* **606**, 785–790 (2022).
24. Lynch, C. J. & Adams, S. H. Branched-chain amino acids in metabolic signalling and insulin resistance. *Nat. Rev. Endocrinol.* **10**, 723–736 (2014).
25. Neinast, M. D. et al. Quantitative Analysis of the Whole-Body Metabolic Fate of Branched-Chain Amino Acids. *Cell Metabol.* **29**, 417–429e4 (2019).
26. patil-et-al-2025. -cinnabarinic-acid-protects-against-metabolic-dysfunction-associated-steatohepatitis-by-activating-aryl
27. Samuel, V. T. & Shulman, G. I. Mechanisms for Insulin Resistance: Common Threads and Missing Links. *Cell* **148**, 852–871 (2012).
28. Hotamisligil, G. S. Inflammation, metaflammation and immunometabolic disorders. *Nature* **542**, 177–185 (2017).

Figures

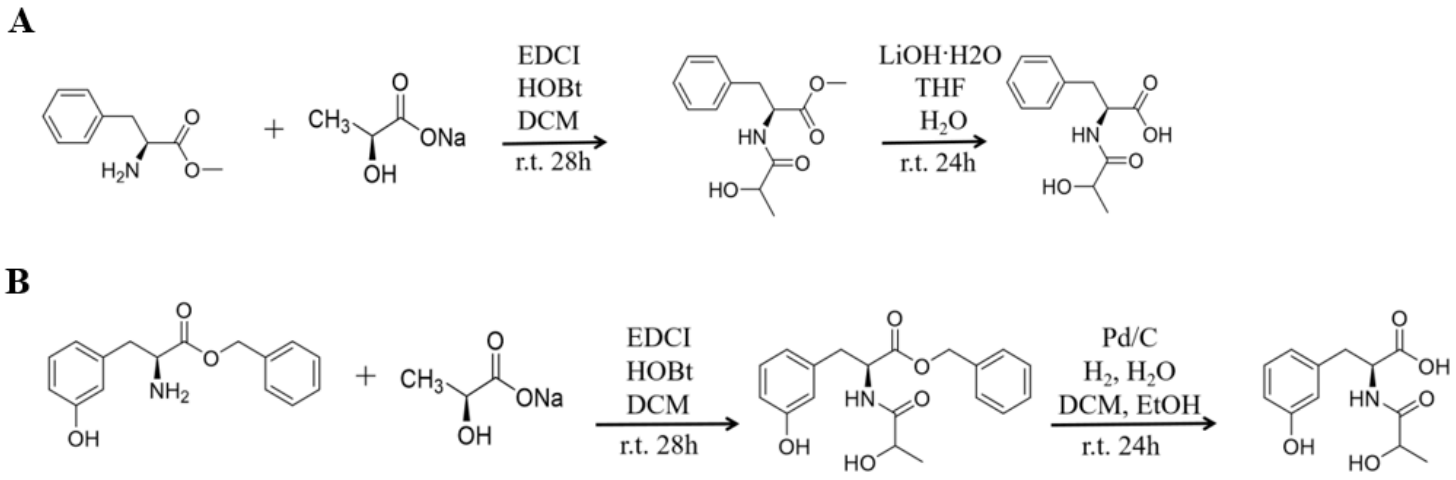

Figure 1

Chemical synthesis routes of (A) Lac-Phe and (B) Lac-Tyr. *EDCI* 1-ethyl-3-(3-dimethylaminopropyl) carbodiimide, *HOBt* 1-hydroxybenzotriazole, *DCM* dichloromethane, *LiOH* lithium hydroxide, *THF* tetrahydrofuran, *EtOH* ethanol

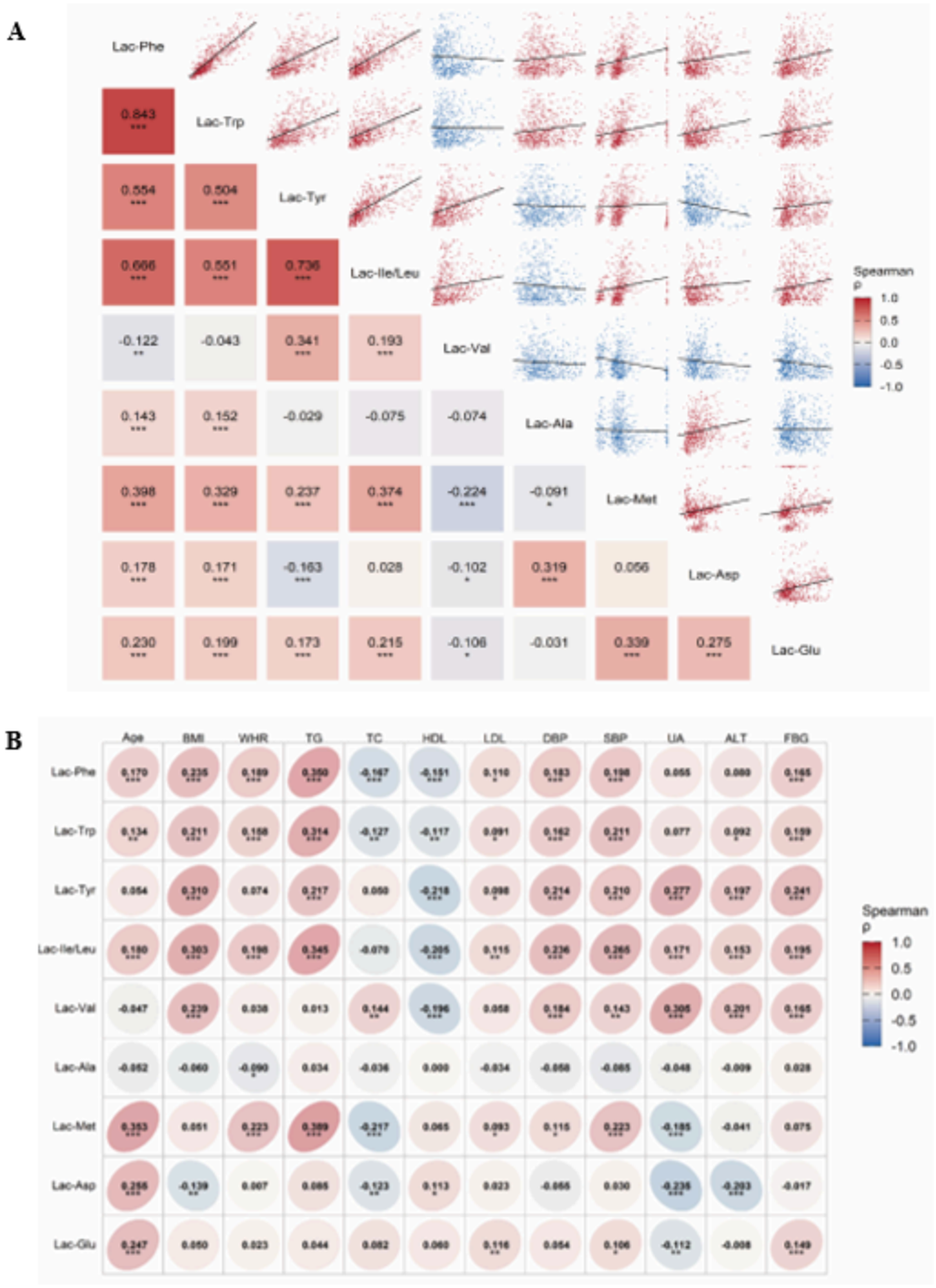

Figure 2

Spearman correlation analysis of the circulating Lac-AAs. (A) Correlations between Lac-AAs and clinical traits. Colored tiles represent ρ values, with ellipses encoding the direction and magnitude of correlation (red,positive; blue, negative). The color scale ranges from −1 to 1, corresponding to ρ values.

Significant levels after Benjamini-Hochberg correction are marked * $p < 0.05$; ** $p < 0.01$; *** $p < 0.001$. **(B) Pairwise correlations among Lac-AAs.** The lower triangle shows correlation coefficients (ρ) as colored tiles; the upper triangle displays corresponding scatterplots with linear regression fits (red,positive; blue,negative).

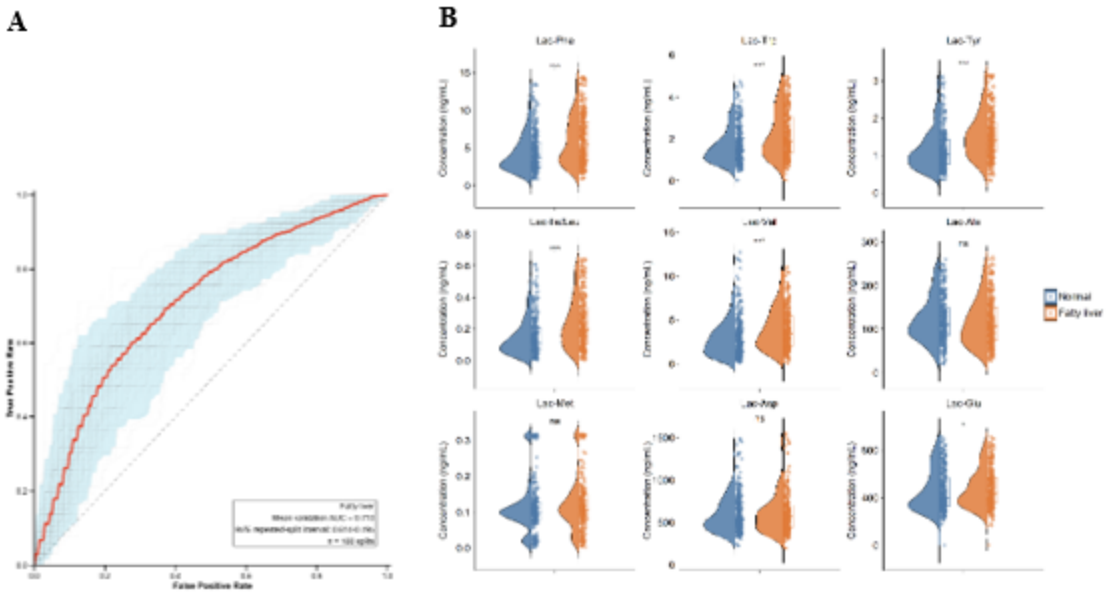

Figure 3

Discriminatory performance of Lac-AAs for Fatty Liver Disease. (A) Serum Lac-AAs concentrations in the Control versus the Fatty Liver groups. *P* values were calculated using the Wilcoxon rank-sum test with FDR adjustment. Significant levels: * $p < 0.05$; ** $p < 0.01$; *** $p < 0.001$; *ns* not significant. **(B) ROC curves derived from Lac-AAs-based logistic models.** Models were built using forward selection in the training cohort and validated in the validation cohort across 100 repeated split iterations. The red line denotes the mean ROC curve across validation runs, and the shaded arearepresents the variability between splits. Mean validation AUC values with 95% repeated-split intervals are also reported.

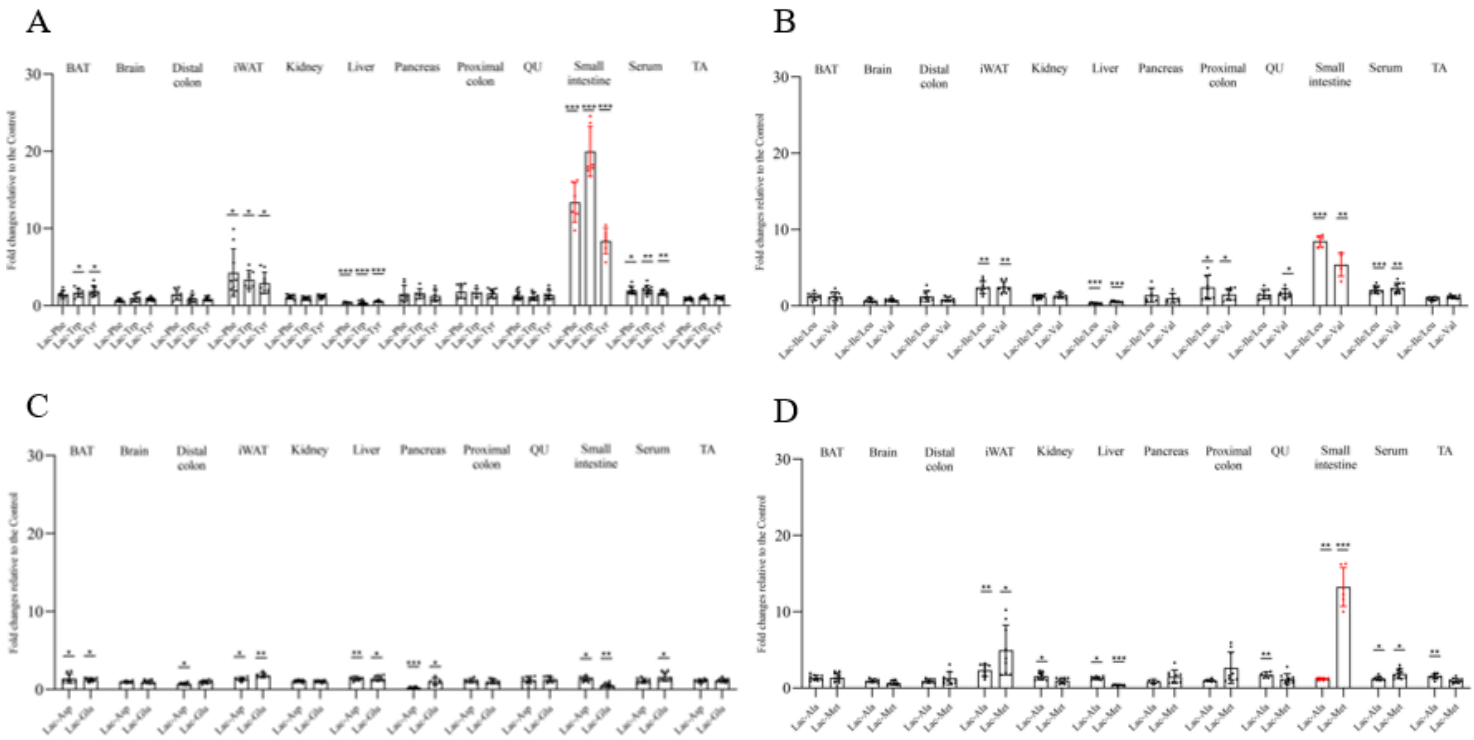

Figure 4

Tissue-specific fold changes in Lac-AAs concentrations between control and fatty liver mice and CNDP2 protein expression in control mice, for (A) Lac-AAAs (Lac-Phe, Lac-Trp, and Lac-Tyr), (B) Lac-BCAAs (Lac-Ile/Leu and Lac-Val), (C) Lac-AAs with negatively charged side chains (Lac-Asp and Lac-Glu), (D) Lac-AAs with hydrophobic side chains (Lac-Ala and Lac-Met). The significant levels: * $p < 0.05$; ** $p < 0.01$; ***$p < 0.001$. *iWAT* white adipose tissue; *BAT* brown adipose tissue; *TA* tibialis anterior muscle, *QU* quadriceps muscle; *Lac-AAAs*lactate-aromatic amino acids; *Lac-BCAAs* lactate-branched-chain amino acids.

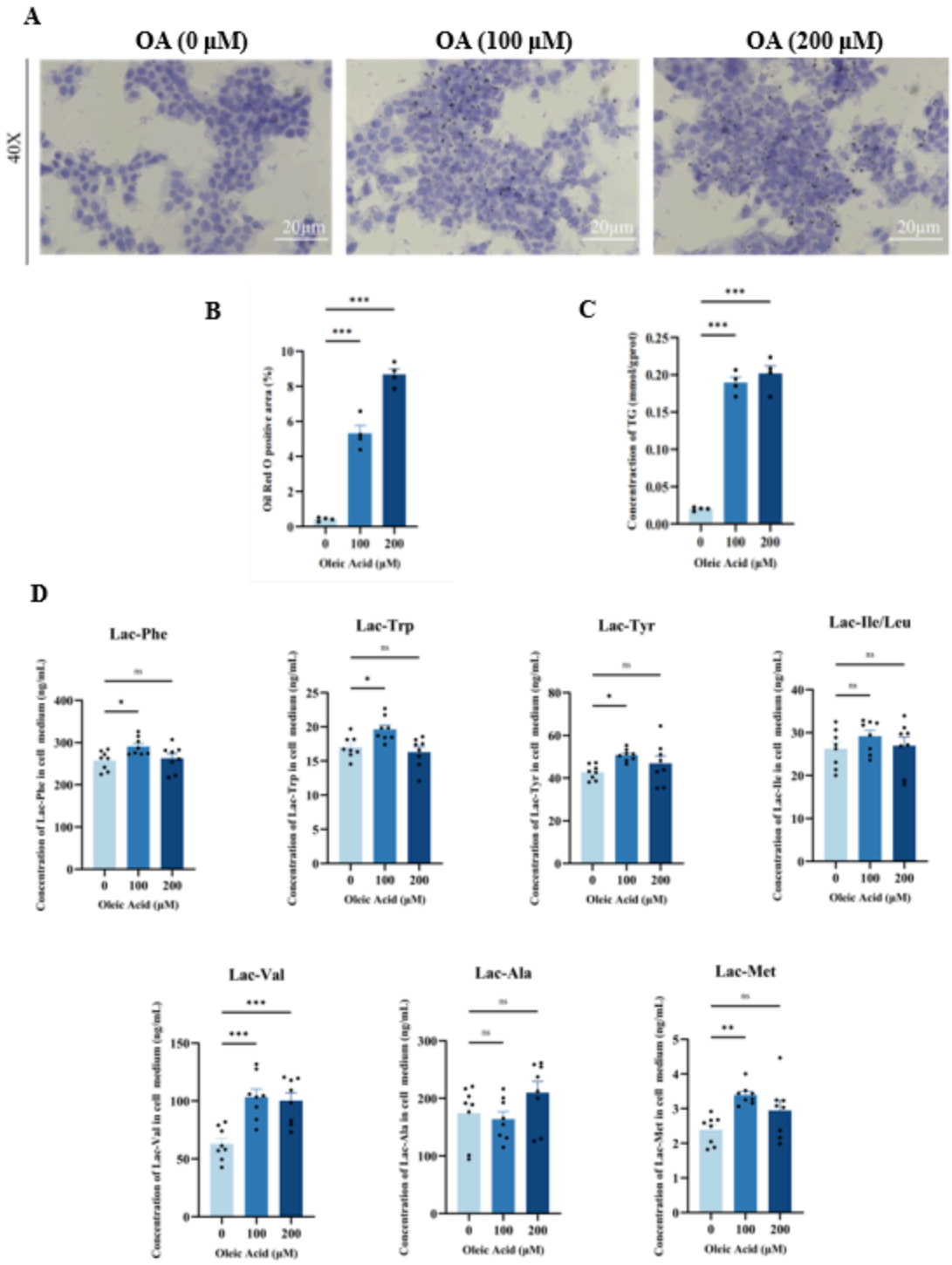

Figure 5

OA-induced lipid accumulation selectively reshapes the Lac-AAs profile in STC-1 cells. (A) Representative Oil Red O staining images (Scale bar = 20 μm); (B) Quantification of the Oil Red O-positive area using ImageJ; (C) Intracellular triglyceride (TG) content, and (D) Extracellular Lac-AAs content in the culture medium of STC-1 cells treated with 0, 100, or 200 μM OA**.** The significant levels: * $p < 0.05$; ** $p < 0.01$; ***$p < 0.001$; ns not significant.

Supplementary Files

This is a list of supplementary files associated with this preprint. Click to download.

- 20261116Supplementarymaterials.docx